



# Investigation into the operation of an autothermal two-section subbituminous coal fluidized bed gasifier

Nikolay Abaimov<sup>1</sup> · Alexander Ryzhkov<sup>1</sup> · Alexey Dubinin<sup>1</sup> · Lu Ding<sup>2</sup> · Vladimir Tuponogov<sup>1</sup> · Sergey Alekseenko<sup>1,3</sup>

Received: 14 November 2022 / Revised: 15 February 2023 / Accepted: 15 May 2023  
© The Author(s) 2023

## Abstract

Using a newly developed experimental setup, the features and advantages of an autothermal single-casing atmospheric subbituminous coal fluidized bed air-blown gasifier, combining a combustion and gasification section, and mixing the dispersed phase (inert material, char) and heat exchange between them through an annular transfer device, have been revealed. To increase the efficiency of the gasifier, an experimental-computational method was developed to find the conditions for optimal operation, combining changing the annular flow's geometry and regulating the primary air for gasification. A simple and reliable multizone thermodynamic calculation model makes it possible to predict the composition of char and syngas in the gasification section with acceptable accuracy. This method confirmed that a two-section fluidized bed gasifier can provide efficient gasification of solid fuels and is suitable for use in small-scale cogeneration plants. Syngas with a heating value of 3.6–4.5 MJ/m<sup>3</sup> and CGE of 38.2%–42.3% was obtained in the experimental setup without optimizing the primary air flow rate. With optimization, the indicators increased to the heating value of syngas of 5.20–5.34 MJ/m<sup>3</sup> and CGE of 42.5%–50.0%. With heat regeneration of 0.8, CGE increases to 70%.

**Keywords** Coal · Syngas · Gasification · Bubbling fluidized bed · Thermodynamics · Modeling

## 1 Introduction

Many modern solid fuel processes involve the thermochemical conversion of coal into syngas. Syngas can be burned (including cogeneration) directly in power plants and converted into liquid fuels in chemical plants.

Three main gasifier designs are common (Meng et al. 2006; You et al. 2018) in small- and medium-sized power plants (up to 25 MW). They are designed to use local fuels, municipal solid waste, and biomass, for embedded generation (Hansen and Bower 2004):

(1) Simple fixed bed gasifiers with counter-current flows that produce syngas with a high content of dust and tar compounds (Luckos and Bunt 2011).

(2) Fixed bed gasifiers with direct flows (inverted gasifiers) that produce high purity gas at a low production rate (Antonelli et al. 2017; Ding et al. 2018, 2022), including pressurized fixed bed gasifier (Ismail et al. 2020).

(3) Fluidized bed gasifiers.

(3.1) Bubbling fluidized bed (BFB) gasifiers that provide high productivity and acceptable syngas quality (Jiao et al. 2021; Figueroa et al. 2017; Du et al. 2021; Jiang et al. 2021; Engelbrecht et al. 2010; Vijay Kumar et al. 2017; Ocampo et al. 2012; Chavan et al. 2012; Tomeczek et al. 1987; Lee et al. 2002; Gupta and De 2022).

(3.2) Spouting fluidized bed (SFB) gasifiers eliminate the use of inert material but require control of oxidizer flow to prevent large fuel carryover (Xiao et al. 2006).

(3.3) Circulating fluidized bed (CFB) gasifiers are more powerful but require more fuel conditioning and capital investment (Ju et al. 2010).

(4) Entrain-flow gasifiers are an alternative higher capacity design developed for integrated gasification combined

✉ Alexander Ryzhkov  
af.ryzhkov@mail.ru

<sup>1</sup> Ural Federal University, Ekaterinburg, Russia 620002

<sup>2</sup> Institute of Clean Coal Technology, East China University of Science and Technology, Shanghai 200237, China

<sup>3</sup> Institute of Thermophysics, Siberian Branch, Russian Academy of Sciences, Novosibirsk, Russia 630090

cycle (IGCC) power plants (Cloete et al. 2018; Ryzhkov et al. 2018) and large chemical plants (Ryzhkov et al. 2016).

(5) Underground gasification units are an alternative to traditional gasifiers, allowing for the production of relatively cheap syngas. However, there is not always a suitable coal seam located near consumers (Wiatowski et al. 2021; Sua et al. 2018).

One of the main advantages of BFB gasifiers is their ability to operate using lignite, sub-bituminous coal (Bläsing and Müller 2013), biomass (Alamia et al. 2017) (including mixed with coal (Zhakupov et al. 2022)), plastics (Du et al. 2021) and some waste (Jiang et al. 2021). These fuels are highly reactive and difficult to finely grind. This makes them ideal for fluidized bed combustion (Emiola-Sadiq et al. 2021). The formation of nitrogen oxides is negligible (Yan et al. 2021) due to the relatively low temperature of the fluidized bed combustion chambers (less than 900 °C). Dry slag removal is also supported. Coal ash containing CaO allows sulfur (Bläsing and Müller 2013) and CO<sub>2</sub> (Kumari and Mohanty 2020) to be retained inside the fluidized bed gasifier. In all the above cases, the coal reacts with an oxidizing gas stream, which typically contains oxygen, nitrogen, carbon dioxide, steam, or some combination of these components. The choice of gas composition is determined mainly by economic feasibility (Hamelinck et al. 2004). Fuel cells can be used to increase plant efficiency (Li et al. 2021).

The optimal operating parameters required to minimize tar emission from coal have been determined in (Matsuoka et al. 2021). A sufficiently high concentration of char almost completely suppresses the formation of heavy and light tar (except for benzene). Figueroa et al. (Figueroa et al. 2017) have optimized the air/fuel ratio in the fluidized bed gasifier, while Ryzhkov et al. (Ryzhkov et al. 2004) analyzed the placement choice of fuel injection in the combustion section.

Heat is required to drive endothermic gasification reactions and maintain the required bed temperature in gasifiers. Heat is generated by the burning part of the syngas, which is generated in one-vessel fluidized bed (BFB-1-1) gasifiers (Leckner 2016). This happens in a dedicated zone inside the fluidized bed (Khan and Wang 2013) or above the reactor headspace (Beenackers and Maniatis 1996). In two-vessel fluidized-bed (BFB-2-1) gasifiers, heat is generated by the burning part of the solid fuel in a separate combustion chamber and transferred to a gasification unit through hot char and inert bed material (Hedenskog 2014; Suárez-Almeida 2021). Combining fuel combustion and char gasification sections into one vessel (BFB-1-2), it becomes technically possible to minimize the dimensions of the installation, CAPEX and maintenance costs, as well as improve the result product's quality. In addition, multistage fluidized bed reactors can capture CO<sub>2</sub> from flue gases (Das 2019).

Khan and Wang (Khan and Wang 2013) studied the operation of a two-section gasifier. This gasifier had a

tube-in-tube design, power of 100 kW, a height of 0.87 m and a diameter of 0.4575 m. The central tube is the combustion section, in which part of the fuel is oxidized to release the heat needed to gasify the fuel fluidized bed in the annular channel (gasification section). The advantage of this technology is a high heating value syngas of 16.64 MJ/kg, design simplicity and the ability to work at existing stations with coal-fired boilers. The disadvantages are the high content of tar in the syngas (64.87%), which will not allow the gas burn in the internal combustion engine, the need to use hot gas cleaning to tar prevent condensation, and a low carbon conversion rate ( $X_C = 0.017\%$ ) and volatiles conversion rate (60.17%), which makes it necessary to burn the produced char in a pulverized coal boiler.

When the sections are arranged vertically rather than horizontally, a two-stage design is obtained. An example is a two-stage subbituminous steam-oxygen gasifier with a 1.34 m spouting bed, which is a special case of a fluidized bed (Tsuji and Uemaki 1994). The lower stage has a smaller diameter (0.114 m) than the upper one (0.2 m), and there is a pinch between them. Large particles are gasified in the lower stage, while fine particles are gasified in the upper stage. Coal enters the lower stage and, after being reduced in size, is carried away by the gas flow to the upper stage, from which syngas exits from the gasifier. A steam-oxygen mixture is supplied to the lower stage, and oxygen to the upper stage. This design's advantages are a wide range of potential fuels, a high carbon conversion rate and CGE. The disadvantages are the gasifier's low capacity and the need for oxygen blast.

Another example of a vertical two-section gasifier is the COORVED gasifier (Laugwitz and Meyer 2014). This gasifier combines a moving bed in the lower section and SFB in the upper section. Such a scheme has the advantages of a moving bed gasifier: optimal heat recovery inside the gasifier and low capital costs, and the advantages of SFB: relatively low specific oxygen demand and high syngas quality. Nevertheless, there are also disadvantages: the need for oxygen blast and steam, and the melting of ash with the agglomeration's formation.

Generating high-quality air-blown gasification syngas for power purposes usually requires either oxygen enrichment of the blast or an additional heat supply. Oxygen enrichment requires an expensive air separation unit and can be used in large power plants such as Nakozo (Kaneko et al. 1997). The heat supply in one-vessel gasifiers is limited by the recuperative heating of the air blast to temperatures of 350–400 °C. When using two-vessel gasifiers, hot ( $\approx 600$  °C) char and air heated (theoretically) up to 350–400 °C are fed into the gasification chamber. When carrying out the conversion in a one-vessel two-section apparatus with a bubbling fluidized bed, it becomes technically possible to increase the air blast's temperature to the char's temperature ( $\approx 700$ – $900$  °C)

and thereby improve the conditions of the process and the syngas's quality (by reducing the amount of RO<sub>2</sub>, tar, and hydrocarbons). This can noticeably raise the cold gas efficiency of the process in the gasification section (CGE<sup>g</sup>):

$$CGE^g = \frac{G_s^g \cdot Q_s^r}{B_c^g \cdot Q_c^r} \approx 100 - d_{slag}, \tag{1}$$

where  $G_s^g$  is syngas flow rate;  $Q_s^r$  is syngas heating value;  $B_c^g$  is char flow rate;  $Q_c^r$  is char heating value;  $d_{slag}$  (< 3%–5%) refers to losses with ash and slag.

In this case, the CGE<sup>u</sup> of the two-section gasifier depends on the syngas heating value and raw fuel characteristics:

$$CGE^u = \frac{G_s^g \cdot Q_s^r}{B_f^u \cdot Q_f^r}, \tag{2}$$

where  $B_f^u$  is fuel flow rate;  $Q_f^r$  is fuel heating value.

The gasifier's operating mode changes depends on the distribution of the air flow rate for combustion and gasification. The fraction of coal in the gasification section ( $s$ ) is equal to the ratio of the cross-sectional areas of the gasification section and the entire gasifier  $s = (d/D)^2$ . When the gasifier operates in the one-section air gasification mode ( $s = 1$ ), it produces a lot of low heating value syngas ( $G_s^g = \max$ ,  $Q_s^r = \min$ ). When the combustion section is separated from the total volume of the gasifier and its volume is increased, the gasification temperature increases, the syngas heating value increases, and the syngas yield decreases, as is shown in Fig. 1.

The  $s$  value characterizes the two most important indicators that determine the gasifier's operational characteristics. On the one hand, the parameter  $(1-s)$  characterizes the area of the annular flow between the upper and lower stages of the combustion section, which controls the quantity and quality (elemental composition) of fuel particles entering the lower part of the gasifier. On the other hand, the  $s$  value determines the proportion of these fuel particles entering the central tube to produce syngas.

This study's aim is to develop a method for finding the optimal operation conditions of a single-casing two-section

autothermal atmospheric subbituminous coal fluidized bed air-blown gasifier with newly developed experimental setup. The change in the parameter  $s$  forms a two-parameter optimization task, which is performed step by step: according to the design parameter  $s$  and according to the regime parameter  $\alpha$  (stoichiometric coefficient).

The present study also aims to demonstrate through experiment and thermodynamic simulation that a two-section fluidized bed gasifier can provide efficient gasification of solid fuels and is suitable for combustion in small-scale cogeneration plants. This could have applications for local energy production, for example, as part of a mini-CHP using piston engines or small-scale gas turbines (Donskoi et al. 2015), based on fuel cells (Dubinin and Shcheklein 2017). In our case, gas cleaning is required since the presence of hydrocarbons causes the formation of highly toxic nitric oxide during gas combustion (Hasegawa 2010). The low heating value syngas cannot easily ignite and burn stably. Tar removal requires expensive equipment, and low heating value syngas enrichment needs additional resources. The advantages of this approach are relatively low CAPEX and simple process conditions.

## 2 Methods and materials

### 2.1 Experiment

To overcome the noted disadvantages of two-sectional gasifiers, a single-casing two-sectional fluidized-bed air-blown gasifier with vertically arranged combustion and gasification sections was developed (Fig. 2). The reactor vessel, made of stainless steel tube, had an internal diameter of 0.273 m at the bottom and 0.5 m at the top. The gasification section is formed by the space below the secondary air inlet plus the inner tube (2). Accordingly, the combustion section is the space above the secondary air inlet in the annular duct. The sections are connected by an overflow annular channel with a limited size. Through this channel, part of the syngas exits to the combustion section, while also the exchanging heat and mass (inert and fuel particles) between the combustion

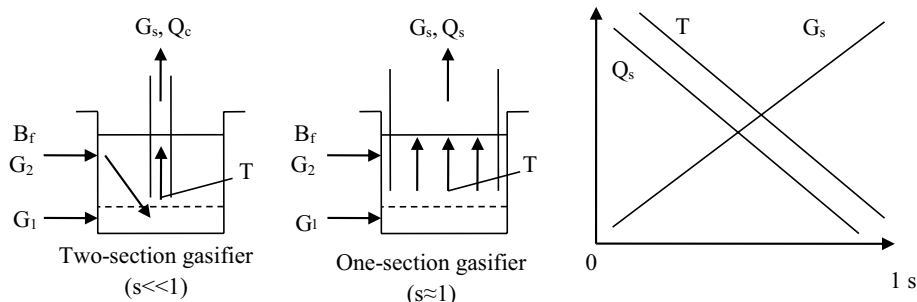


Fig. 1 Effect of sectioning on the gasifier

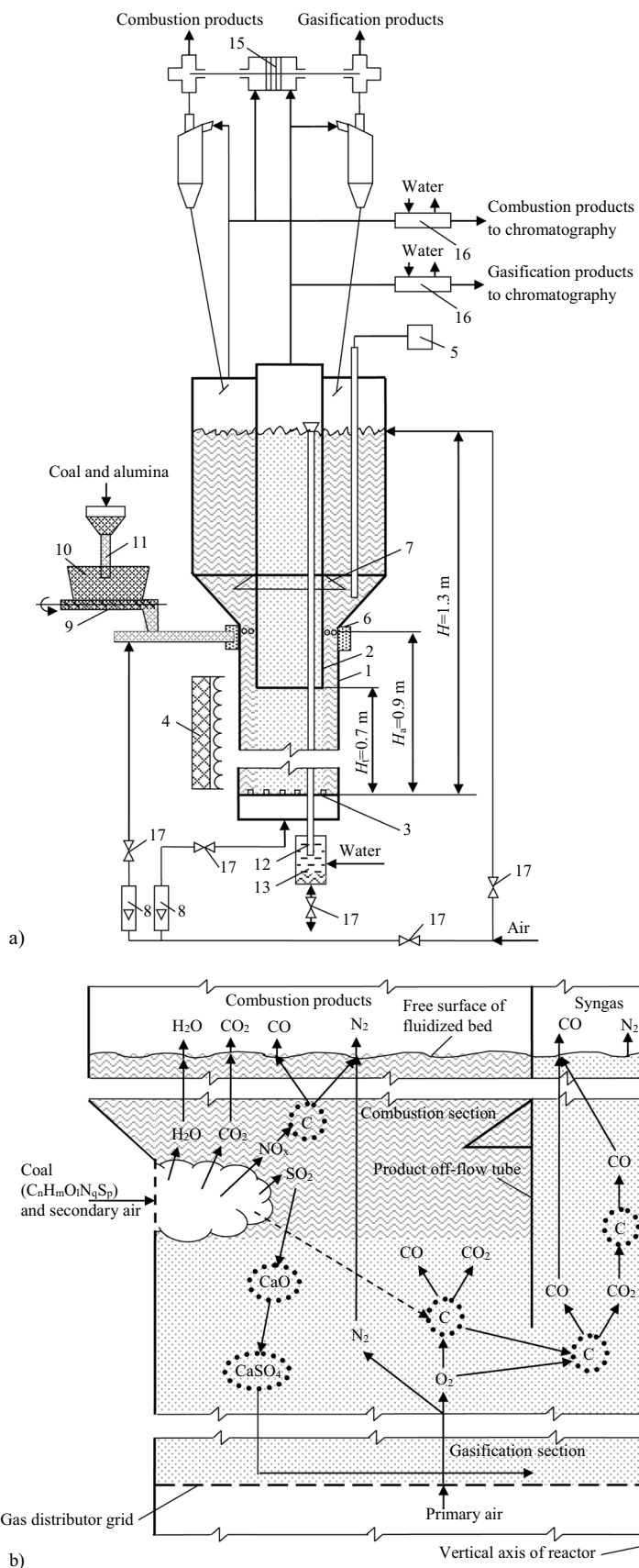


Fig. 2 Diagrams: a gasifier design; b reaction scheme

and gasification sections. The central tube's lower end has a height of 0.7 m from the gas distribution grid. This height was selected as a result of a search to ensure the syngas heating value is at maximum. A mixture of inert material (aluminum oxide) is loaded into the gasifier, after which air is supplied through the gas distribution grid (3); the bed is heated by an external electric heater (4). After reaching the temperature regime, coal is supplied. The combustion section bed temperature is controlled by a chromel–alumel thermocouple (5). The electric heater heating the gasifier is switched off in the steady state coal gasification mode when a bed temperature of 700 °C is reached. The gasification products (syngas) entering the inner tube (2) and immersing in the bed are removed from the gasifier. To control the bed temperature in gasification mode, the remaining part of the syngas is burned in an annular bed between the gasifier external wall and the inner tube (2), where secondary air and a mixture of crushed and screened coal with inert material are also supplied through the feeder's holes (6). A turbulator (7) was installed on the inner tube to intensify the mixing of air and volatile matter. The air flow rate is controlled by rotameters (8), and the mixture of coal and inert material is controlled by a screw feeder (9). A constant bed height in the gasifier (1.3 m) is ensured by the removal of ash and inert aluminum particles through a draintube (12) with a water seal (13). The combustion products emerging from the annular space between the inner tube and the gasifier's external wall are mixed with tertiary air to burn off the residual carbon monoxide. The proportion of syngas withdrawn from the gasifier through the central tube  $s$  is determined by the ratio of the gasification section's cross-sectional areas and the entire gasifier  $s = (d/D)^2$ . In the experiments stainless steel tubes with a wall thickness of 1 mm and an internal diameter ( $d$ ) of 0.227 m, 0.236 m and 0.262 m, corresponding to  $s$  values of 0.69, 0.75 and 0.92 were used. Thus, the combustion section was connected to the gasification section by a narrow, slot-like annular channel 0.2 m high and 4 to 20 mm wide, which significantly affected the circulation of fuel and inert particles between the sections and the residence time of fuel particles in the combustion section. If the channel width is changed, the volume and composition of the syngas leaving the inner tube will change. With the use of a narrow channel, the downward movement of the heated particles becomes more difficult, while the residence time of fuel particles in the combustion section and the degree of their conversion increase. If such particles enter the gasification section, the syngas will be free of hydrocarbon pyrolysis products. However, in extreme cases, the use of a narrow channel can block the downward movement of the particles, and the fuel supply to the gasification section will stop. The continued operation of the gasifier in this case is possible by moving the fuel supply point to the bottom of the gasifier, as is done in the previously mentioned two-stage plant (Tsuiji

and Uemaki 1994). With the use of a wider channel and improved communication between the sections, the downward movement of the inert and fuel particles increases; however, the residence time of the fuel particles from the combustion section will decrease, as will the conversion degree. In an extreme case, a scenario arises when unpyrolyzed particles are supplied to the gasification section, which will lead to the production of syngas ballasted with tars, as in the previously mentioned two-section technology (Khan and Wang 2013). Changes in the qualitative composition and quantitative characteristics of the particles entering the gasification section will be reflected in the demand for air volumes supplied to the gasification section. Running the gasifier with no tube corresponds to  $s = 1$ . The combustion products from the annular space (combustion section) and syngas from the central tube (gasification section) are removed from the gasifier through separate cyclones (14). The cyclones are connected hydraulically to a pressure regulator (8) in order to maintain near atmospheric pressure and equalize the bed levels in the central tube and the annular space. Gas sampling uses gas removal from the cyclones with water-cooled tubes (16). The composition of the samples was determined on a Gasochrome 3101 chromatograph with a relative measurement error of 5%.

The fuel used was subbituminous Borodino coal with a particle size distribution typical of bubble fluidization (Fig. 2). Belonging to group B according to the Geldart classification, this material forms a stationary bubbling fluidized bed when blown at relatively low velocities ( $< 3$  m/s). Well-flowing corundum powder with a density of 3760 kg/m<sup>3</sup> and an average particle size of 0.32 mm, close to the average particle size of the coal, was used as an inert bed material. The primary air superficial velocity of  $u = 0.24$  m/s (for the entire section of the setup) was set to be lower than the minimum fluidization velocity of  $u_{mf} = 0.267$  m/s, which made it possible to reduce entrainment during gas expansion in the working hot mode while maintaining intense heat and mass transfer. The velocities are calculated under normal conditions (Fig. 3).

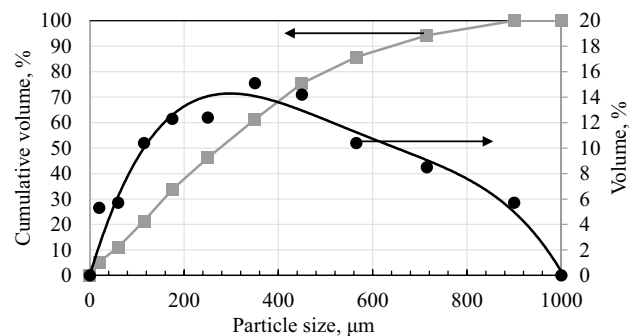


Fig. 3 Particle size distribution of the Borodinsky coal

In operating mode (900 °C), the velocity of the hot air increases to 0.96 m/s. The minimum fluidization velocity of  $u_{mf}$  for corundum particles will decrease to 0.12 m/s, while for coke particles  $d = 1$  mm minimum fluidization velocity will be 0.2 m/s. In this mode, the inert material and fuel particles will be intensively mixed by gas bubbles. This explains the equalization of the temperature over the volume of the gasifier's sections and the diffusion flow of non-volatile carbon particles from the place where coal is loaded to the place where the char is unloaded in the gasification section (in our plant diagram unloading (drain) is at the top).

The actual velocity of the conversion products leaving the fluidized bed due to gas formation will be somewhat higher than that of hot air, but still less than the terminal (free-fall) velocity of isolated corundum particle (0.32 mm  $u_t = 3.5$  m/s). However, the smallest particles of fuel and inert material will be picked up by the flow, carried out of the gasifier into the cyclone.

The characteristics of the supplied coal are given in Table 1, the operating conditions of the gasifier in Table 2, and the experimental program in Table 3.

As shown in Fig. 2b, at the level of the secondary air and coal supply point, the newly formed gases are carried away by the gas flow upwards, while char and ash particles move downward towards the gas distribution grid. The temperature at the exit from the combustion zone approaches the temperature of the fluidized bed (700–900 °C). This contributes to the development of adverse reactions (Wang et al. 2020). Some of the resulting products from the adverse reactions ( $\text{NO}_x$ ,  $\text{SO}_2$ ,  $\text{CO}_2$ ) interact with char and ash particles, as shown in Eqs. (3) and (4) (Pérez-Astray et al. 2019; Ding et al. 2015), with the formation of  $\text{N}_2$ ,  $\text{CO}$ ,  $\text{CaSO}_4$ :

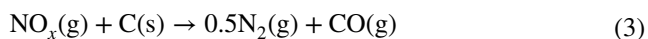


**Table 1** Ultimate and proximate analysis of Borodinskiy coal and ash composition

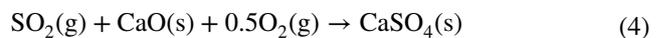
Parameter	Value	Parameter	Value
LHV (MJ/kg)	19.34	$\text{SiO}_2$ (%)	46.8
W (%)	12.0	$\text{Al}_2\text{O}_3$ (%)	12.9
A (%)	9.7	$\text{TiO}_2$ (%)	0.6
C (%)	55.9	$\text{Fe}_2\text{O}_3$ (%)	7.9
H (%)	3.9	CaO (%)	25.8
N (%)	1.1	MgO (%)	5
O (%)	17.3	$\text{K}_2\text{O}$ (%)	0.5
S (%)	0.2	$\text{Na}_2\text{O}$ (%)	0.5
$V^{\text{daf}}$ (%)	47	Slagging start temperature (°C)	950

**Table 2** Gasifier operating conditions

Parameter	Value
Coke bed concentration	0.1 kg on 1 kg of mixture
Coke mean particle diameter	$1 \times 10^{-3}$ m
Density of coke	1650 kg/m <sup>3</sup>
Alumina mean particle diameter	$0.32 \times 10^{-3}$ m
Density of alumina	3760 kg/m <sup>3</sup>
Voidage at minimum fluidization	0.48
Total bed height	1.3 m
Secondary air and coal supply height	0.9 m

**Table 3** Program of experiments

s	d(m)	Coal flow rate B (kg/h)	Primary air flow rate $V_1$ (m <sup>3</sup> /h)	Secondary air flow rate $V_2$ (m <sup>3</sup> /h)	Total air flow rate, (m <sup>3</sup> /h)
0.69	0.227	25.4	50	65.60	115.60
0.75	0.236	25.4	50	63.20	113.20
0.92	0.262	25.4	50	57.55	107.55
1	None	25.4	50	0	50



The ash particles, together with the captured sulfur, are removed from gasifier in the upper part of the gasification section. The total gas flow is distributed between the gasification section and the combustion section in the proportion:  $s = (d/D)^2$ —and  $(1-s)$ , respectively.

## 2.2 Modelling

As described in the previous section, several reaction zones are formed in the two-section gasifier. Two main zones can be distinguished—the gasification zone and the combustion zone. These zones do not directly correspond to the sections. Therefore, a multizone thermodynamic model has been developed to calculate the operation parameters. Similar models apply to one-section gasifiers (Biagini et al 2016). However, a two-section gasifier has its own specifics in the form of two separate gas outlets (syngas and combustion products).

The developed model is based on the following assumptions. The gasifier operates in steady state at a pressure of 101.13 kPa. The residence time of the reactants inside the gasifier is sufficient to achieve chemical equilibrium under adiabatic conditions. The supply air is dry at 25 °C and 101.13 kPa. Ash reaction is not considered. Syngas is an ideal gas consisting of  $\text{CO}$ ,  $\text{CO}_2$ ,  $\text{H}_2$ ,  $\text{CH}_4$ ,  $\text{H}_2\text{O}$ , and  $\text{N}_2$ . The combustion products consist of  $\text{CO}_2$ ,  $\text{H}_2\text{O}$ ,  $\text{N}_2$ , and  $\text{O}_2$ . The coal and char contain C, H, N, O, S,  $\text{H}_2\text{O}$ , ash (inert).

This calculation method has been applied to determine the compositions of the syngas, char and combustion products. The complex of calculations is performed according to the following algorithm:

- (1) determination of the composition of the reagents in the gasification section, which allows for obtaining the composition of syngas as in the experiment;
- (2) excretion of the composition of the char in the gasification section from the reagents composition (a mixture of air and char);
- (3) calculation of the composition of the reagents in the combustion section based on the composition of the char in the gasification section;
- (4) calculation of the composition of the combustion products in the combustion section based on the reagent composition.

Char composition is determined based on the following conditions:

- (1) in the gasification section, only char is gasified, without impurities of raw coal;
- (2) there is no moisture in the char;
- (3) the main components of the char are fixed carbon and ash; volatile matter is the smallest part.

The equilibrium composition of the reaction products is calculated by the entropy maximization method (EMM). A detailed description of the practical implementation of this method and its verification are presented in (Gorokhovski et al. 2005; Messerle et al. 2017).

It follows from the laws of thermodynamics that in a state of equilibrium, an isolated system's entropy is maximum. Therefore, the problem of calculating equilibrium composition can be reduced to finding the coordinates of the conditional entropy maximum. The principle of maximum entropy is valid for any equilibrium system, regardless of the path along which the system reached equilibrium (according to the second law of thermodynamics):

$$S = \sum_{i=1}^k S_i^{(p_i)} \cdot n_i + \sum_{l=1}^L S_l \cdot n_l = \sum_{i=1}^k (S_i^0 - R_0 \ln \frac{R_0 T n_i}{v}) \cdot n_i + \sum_{l=1}^L S_l^0 \cdot n_l, \tag{5}$$

where  $S$  is entropy (J/(kg K));  $S_i^{(p_i)}$  is entropy of the  $i$ -th component of the gas phase (J/(mol K)) at the partial pressure of its equilibrium state  $p_i = R_0 T n_i / v$  (Pa);  $n_i$  is content of the  $i$ -th gaseous component in the system (mol/kg);  $S_l$  is entropy of the condensed phase  $l$ , which depends only on temperature;  $v$  is the specific volume of the system;  $S_i^0$  is standard entropy of the  $i$ -th component of the gas phase at temperature  $T$  and

pressure 0.1 MPa; and  $R_0$  is universal gas constant (J/(mol K)).

The determination of the parameters of the equilibrium state consists of finding the values of all dependent variables, including the numbers of moles of the components and phases, at which the value of  $S$  reaches its maximum. When finding an extremum, additional connections are imposed on the values of the unknown unknowns, reflecting the conditions for the system's existence: the constancy of the total internal energy, as for the system is isolated, the constancy of the mass of chemical elements, as for a closed system, and the general electroneutrality:

$$-U + \sum_{i=1}^{k+L} U_i \cdot n_i = 0; b_j = \sum_{i=1}^{k+L} a_{ji} n_i, j = 1, 2, \dots, m; \sum_{i=1}^k a_{ei} n_i = 0, \tag{6}$$

where  $U$  is internal energy (J/(kg K));  $U_i$  is internal energy of the  $i$ th component (J/mol K);  $a_{ji}$  is stoichiometric coefficients;  $m$  is the number of chemical elements in the system; and  $b_j$  is the content of the  $j$ -th element in the system.

As a result, finding the composition and properties of arbitrary composition corresponding to the state of the maximum entropy of a conditionally isolated system is required to solve a nonlinear system of Eqs. (7–11):

$$G_i - R_0 \ln \frac{R_0 T}{v} - R_0 \ln n_i + \sum_{j=1}^m a_{ji} \lambda_j + a_{ei} \lambda_e = 0, (i = 1, 2, \dots, k); \tag{7}$$

$$\left( G_l + \sum_{j=1}^m a_{jl} \lambda_j \right) \cdot n_l = 0, (l = 1, 2, \dots, L); \tag{8}$$

$$\sum_{i=1}^{k+L} a_{ji} n_i - b_j = 0, (j = 1, 2, \dots, m); \tag{9}$$

$$\sum_{i=1}^k a_{ei} n_i = 0; \tag{10}$$

$$R_0 T \sum_{i=1}^k n_i - p v = 0; \tag{11}$$

$$\sum_{i=1}^{k+L} U_i n_i - U = 0, \tag{12}$$

where  $G_i$  is Gibbs energy of the  $i$ -th component (J/(mol K));  $\lambda_j$  is the Lagrange multiplier of the  $j$ -th component.

This system is solved iteratively. The thermochemical and thermodynamic characteristics of individual substances are taken from (JANAF 1985).

The equilibrium composition of the reaction products almost does not contain methane. However, the rate of its decomposition is quite low. Therefore, in the calculation it is assumed that methane is equal to the experimentally obtained values.

Coal with a known composition is supplied to the combustion section; however, it is not coal that enters the gasification section, but the product of its conversion—char with an unknown composition, which varies depending on  $\alpha$  and  $s$ . To determine the composition of char in the gasification section, thermodynamic calculations were carried out according to the algorithm shown in Fig. 4.

### 3 Results and discussion

#### 3.1 Char composition

The experiment was carried out with  $s=0.69-1$ , but the calculation was carried out with  $s=0-1$  in order to get a complete picture of the dependence of the gasifier parameters on  $s$ . As seen in Fig. 4, the composition of the syngas is determined based on char composition, so determining this parameter is a paramount task. Char composition for cases with  $s < 0.69$  was determined by extrapolation of the data obtained for  $s > 0.69$ .

Char composition is shown in Fig. 5. In the case of  $s = 1$ , there was no gasification section; that is, syngas was produced not from char, but from coal. Therefore, the figure for  $s = 1$  shows not the composition of the char, but the composition of the reacting part of the coal ( $X_C \approx 40\%$ ). The second extreme point is mode  $s = 0$ , which was not in the experiment, unlike  $s = 1$ . In this

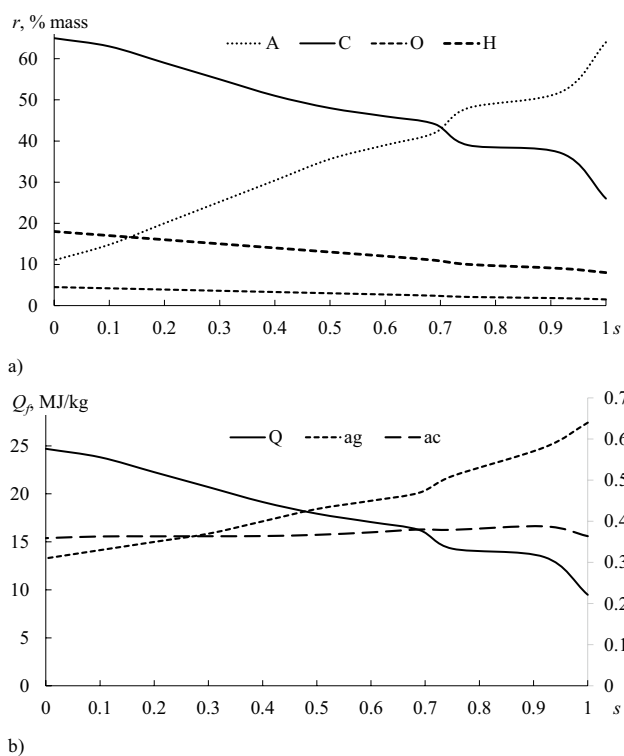


Fig. 5 a Char composition; b Heating value and  $\alpha$

mode ( $s = 0$ ), there is no gasification section, and the syngas consumption is zero; therefore,  $s = 0.001$  is taken as the extreme point for calculations. At this extreme point, the carbon content in the char is maximum and the ash content minimal; that is, char composition is as close

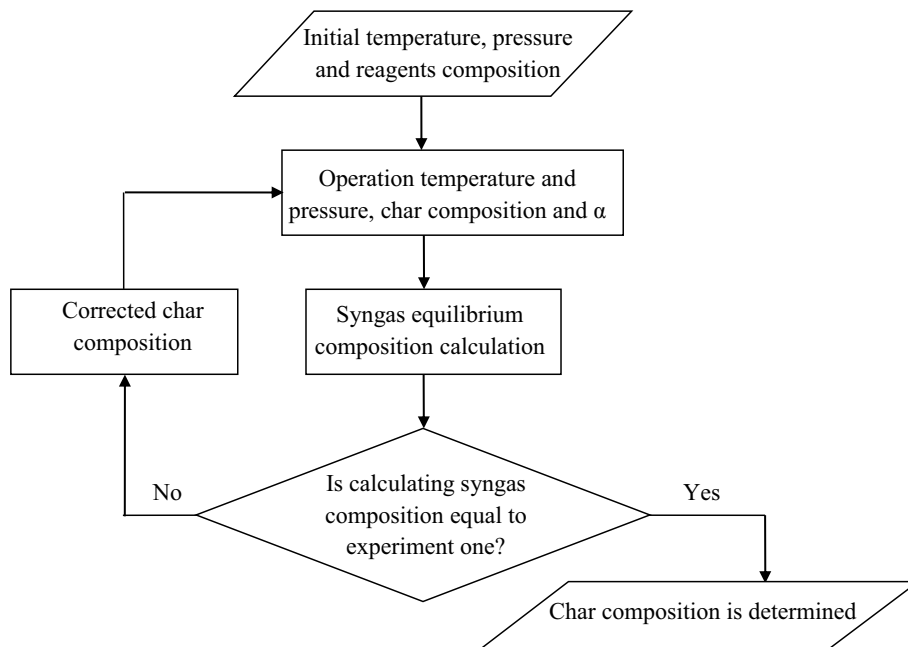


Fig. 4 Algorithm for determining char composition

as possible to coal composition. In the case of  $s \rightarrow 1$ , the exchange between the combustion and gasification sections becomes more difficult, while the residence time of the fuel particles in the combustion section and the degree of pyrolysis increase. In this mode, the amount of carbon in the char, as well as H and O is minimal. Conversely, with a decrease in  $s$  and an improvement in the connection between the combustion and gasification sections, the residence time of fuel particles in the combustion section decreases, as does the degree of pyrolysis. This logic is reflected in Fig. 1. The char heating value is defined as:

$$Q_f = \frac{339 \cdot C + 1025 \cdot H - 108.5 \cdot O}{1000} \tag{13}$$

With the increase of  $s$ , the ash content in the char increases and the content of volatile matter decreases since fuel with a higher degree of burnup from the combustion section enters the gasification section. At the same time,  $\alpha_g$  increases, since the air flow rate remains unchanged, and the amount of combustibles in the char decreases, which leads to a decrease in the syngas heating value, as shown below. To calculate  $\alpha_g$ , the equation is applied:

$$\alpha_g = \frac{0.0889 \cdot C + 0.265 \cdot H - 0.0333 \cdot O}{V_1 \cdot B} \tag{14}$$

To determine the mode of coking on the graph,  $\alpha_c$  is  $\alpha$  carbonization was plotted, calculated by the formula:

$$\alpha_c = \frac{\frac{C}{12} - \left(\frac{2 \cdot O}{16} + \frac{W}{18}\right)}{\frac{2 \cdot C}{12} + 0.5 \cdot \left(\frac{H}{1} + \frac{2 \cdot W}{18}\right) - \left(\frac{2 \cdot O}{16} + \frac{W}{18}\right)} \tag{15}$$

At  $s < 0.3$   $\alpha_g < \alpha_c$ , free carbon forms in the system.

### 3.2 Syngas composition

The experimental and EMM syngas compositions for different values of  $s$  are shown in Fig. 6. Nitrogen is not shown in the graph for convenience. The syngas heating value is determined by the equation:

$$Q_s^g = \frac{12.63 \cdot r_{CO} + 10.78 \cdot r_{H_2} + 35.83 \cdot r_{CH_4}}{100} \tag{16}$$

where  $r$  is the amount of gases in the synthesis gas (% vol).

CGE is calculated by the equation:

$$CGE = \frac{Q_s^r \cdot \left(s \cdot V_1 \cdot \frac{r_{N_2}^a}{r_{N_2}^s}\right)}{Q_f^r \cdot B} \tag{17}$$

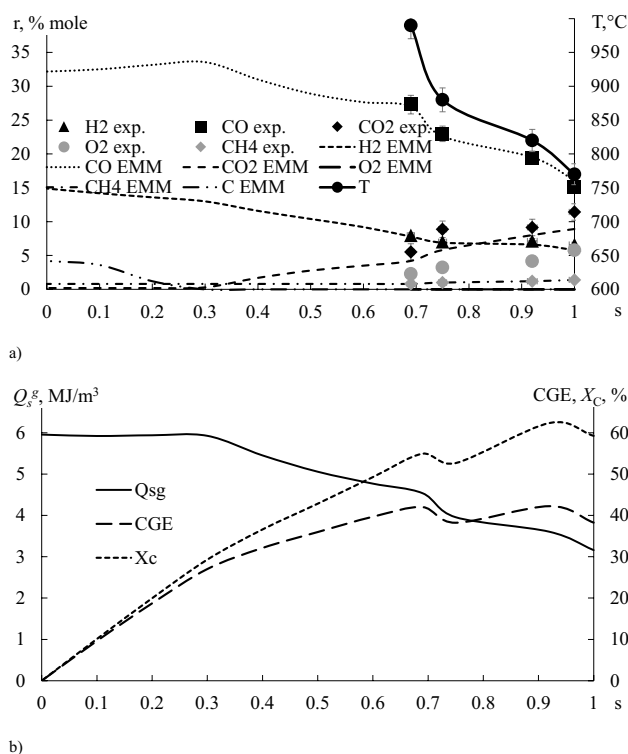


Fig. 6 a Experimental and EMM syngas composition; b Heating value, CGE and  $X_c$

where  $Q_s^r$  is the syngas heating value (MJ/m<sup>3</sup>);  $V_1$  is primary air flow rate (m<sup>3</sup>/h);  $r_{N_2}$  is nitrogen in syngas (% vol.);  $r_{N_2}^a$  is nitrogen in air, %,  $r_{N_2}^a = 79\%$ ;  $Q_f$  is coal heating value (MJ/kg);  $B$  is coal flow rate (kg/h). This equation is suitable for calculating the conversion of coal with a low nitrogen content, in our case 1.1%. To calculate  $X_c$ , the equation is used:

$$X_c = \frac{s \cdot V_1 \cdot \frac{r_{N_2}^a}{r_{N_2}^s} \cdot M(C) \cdot (r_{CO} + r_{CO_2} + r_{CH_4})}{C \cdot v \cdot B \cdot 100} \tag{18}$$

where  $M(C)$  is the carbon molar mass,  $M(C) = 12$  kg/kmol;  $v$  is molar volume of ideal gas,  $v = 22.4$  m<sup>3</sup>/kmol;  $B$  is coal flow rate,  $B = 25.4$  kg/h.

From the figure, we see that in the experimental range  $s = 0.69-1$ , as  $s$  increases, the temperature drops from 990 to 770 °C, which is explained by an increase in the total  $\alpha$  and cooling of the layer by excess cold air. In the calculated range  $s = 0-0.69$ , the temperature was set at 990 °C as in the experimental mode  $s = 0.69$ , in which the total  $\alpha = 1$ . At the same time, the concentrations of the combustible components of the syngas also fall, which is explained by a decrease in the amount of volatile substances in the char. At  $s < 0.3$ , free carbon appears in the system (due to  $\alpha_g < \alpha_c$ ), so the CO concentration starts to decrease. The composition of the resulting syngas is typical for coal gasifiers, but the

heating value exceeds the heating value of some biomass gasifiers syngas by 30% (Figuroa et al. 2017).

CGE in the experiment ranges from 38.2% to 42.3%, although the heating value decreases as  $s$  increases from 4.7 to 3.2 MJ/m<sup>3</sup>. This is because with an increase in  $s$ , the yield of syngas increases in direct proportion, which increases CGE. Syngas with this heating value can be used as fuel for internal combustion engines (Castro et al 2022). The non-monotonicity of CGE and its peak at  $s=0.69$  is explained by the maximum temperature of the process, which leads to an increase in the rates of all reactions in the experiment. At  $s < 0.3$ , the reagent gases become insufficient for complete carbon gasification, which leads to a constant syngas heating value in this range. Therefore, it makes no sense to reduce  $s$  below 0.3, since the heating value will not exceed 6 MJ/m<sup>3</sup>.

A maximum CGE of 42.3% is achieved at  $s=0.92$ , however, this mode has a minimum heating value of 3.6 MJ/m<sup>3</sup>, which must be taken into account when using this syngas as a fuel for internal combustion engines or small-scale gas turbines.

When analyzing  $X_C$ , it can be seen that its change is similar to the change in CGE. With optimal  $s=0.92$ , the  $X_C$  parameter is 62%. This means that 48% of the carbon converts to the combustion products CO<sub>2</sub> and to the unburnt char in the combustion section. In the limiting case  $s=1$ , the  $X_C$  parameter is 60%. However, in this case, there is no separation into sections and all the formed CO<sub>2</sub> is in the syngas, as well as the entire unburnt char is in one section.

In addition, this simulation makes it possible to determine the concentration of harmful emissions: H<sub>2</sub>S = 0.04%, NO<sub>x</sub> = 5 ppm. However, it is known that calcium in ash binds sulfur compounds (Bläsing and Müller 2013). The high concentration of CO<sub>2</sub> and the reducing atmosphere of the reaction decrease the release of nitrogen oxides (Ma et al. 2021). The high Ca/S ratio of coal (6.8) also indicates the low amount of sulfur compounds (Dubinin et al. 2021; Sheng et al. 2000) and nitrogen oxides (Xiaorui et al. 2021) in the resulting syngas. The inclusion of calcium in the thermodynamic calculation will make it possible to clarify the concentration of harmful substances.

### 3.3 Influence of temperature on the syngas composition

The gasification temperature in the fluidized bed is limited on the one hand by the temperature required for sufficient rates of chemical reactions (about 700 °C), and on the other by the temperature of the start of slagging (about 1000 °C). In this temperature range, the composition of the syngas was calculated at  $s=0.92$ . The dependence of syngas composition on temperature is shown in Fig. 7.

It can be seen from the figure that as the temperature increases, the concentrations of CO and H<sub>2</sub>O increase,

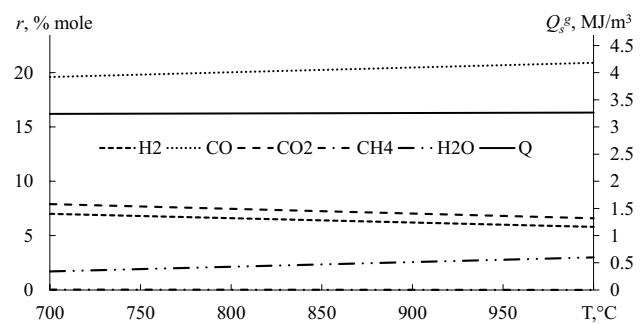


Fig. 7 Dependence of syngas composition on temperature

while those of CO<sub>2</sub> and H<sub>2</sub> decrease. This is due to the equilibrium shift in the water gas shift reaction. At the same time, the heating value practically does not change. Obviously, an increase in temperature leads to an increase in the rate of chemical reactions and the degree of fuel conversion rate, but the thermodynamic model used does not take into account kinetic limitations. Lowering the process temperature can be beneficial when it is necessary to increase the H<sub>2</sub>/CO ratio in the syngas (in chemical plants or in CO<sub>2</sub> capture and storage).

### 3.4 Influence of primary air flow

In order to prevent the decrease in the syngas heating value at  $s > 0.3$  and the formation of free carbon at  $s < 0.3$ , it is necessary to supply the primary air flow with  $\alpha_c$ , i.e. increase the gas velocity more than 0.24 m/s at  $s < 0.3$  and, vice versa, decrease it at  $s > 0.3$ . Figure 8a shows the air velocities in the installation, reduced to stoichiometric gasification air flow rates under the grate, depending on  $s$  at temperatures of 20 and 900 °C. For cold air, only at  $s \rightarrow 0$  does the air velocity increase to a value of minimum fluidization velocity  $u_{mf} = 0.267$  m/s. In the operating mode, at an air temperature of 900 °C, the air velocity is in the range of 0.536–1.1 m/s ( $\frac{u}{u_{mf}} = 4.5\text{--}9.1$ —the mode of developed bubble fluidization) and does not reach the terminal velocity of corundum particle  $u_t = 3.5$  m/s and coke particles of 7.4 m/s. At  $\alpha_c$ , synthesis gas consists of H<sub>2</sub>, CO, and N<sub>2</sub>, since there is not enough oxygen to form H<sub>2</sub>O and CO<sub>2</sub>. The composition of the syngas (Fig. 8b) changes insignificantly—H<sub>2</sub>—10–14%, CO—34–32%,  $Q_s^g$ —5.2–5.7 MJ/m<sup>3</sup> (Fig. 8c). Syngas with such a heating value is widely used for combustion in internal combustion engines (Perrone et al. 2023). The maximum is more pronounced. CGE increases by almost 8% and reaches 50%, which indicates the expediency of a fine selection of primary air flow. At the same time, thermodynamic calculations of the equilibrium composition of syngas were

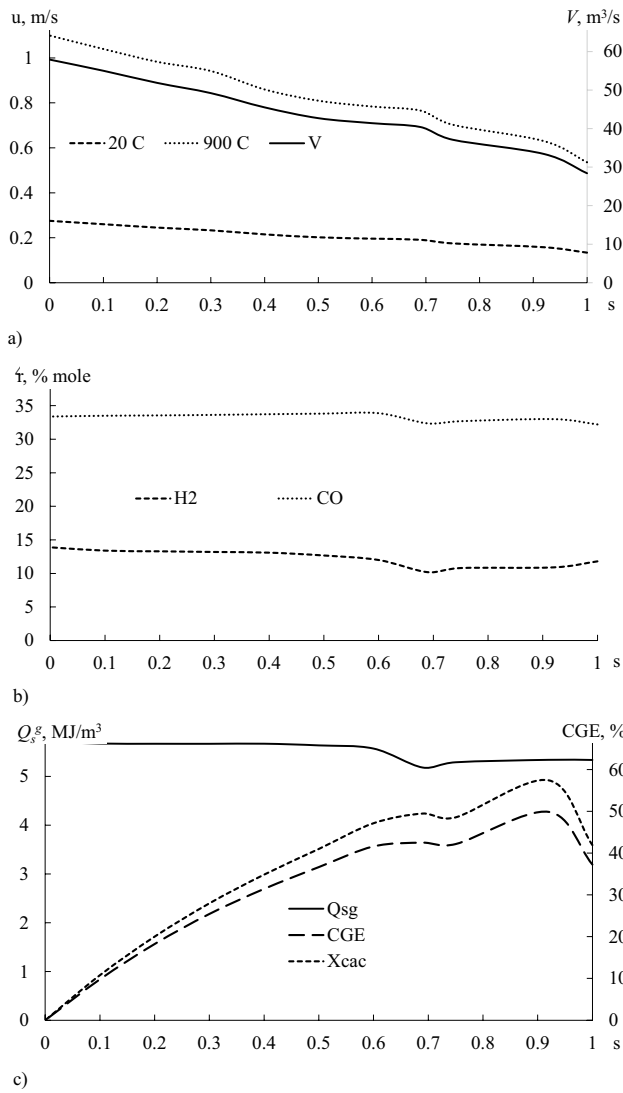


Fig. 8 Influence of primary air flow rate

carried out without taking into account the kinetics of chemical reactions; accordingly, the results are idealized. In a real installation, not all oxygen can react with the fuel, so  $\alpha_g$  must be greater than  $\alpha_c$ . Therefore, further studies are planned using the CFD method and taking into account the kinetic features of the process.  $X_C$  with  $\alpha_c$  is calculated by the equation:

$$X_C^{\alpha_c} = \frac{s \cdot V_1 \cdot \frac{\alpha_c}{\alpha_g} \cdot \frac{r_{N_2}^a}{r_{N_2}} \cdot M(C) \cdot (r_{CO} + r_{CO_2} + r_{CH_4})}{C \cdot v \cdot B \cdot 100} \quad (19)$$

### 3.5 Effect of regeneration on CGE

The gasifier CGE at different  $s$  is obtained using the syngas yield  $2.08 \text{ m}^3$  of gas per kg of coal on a dry basis. This value

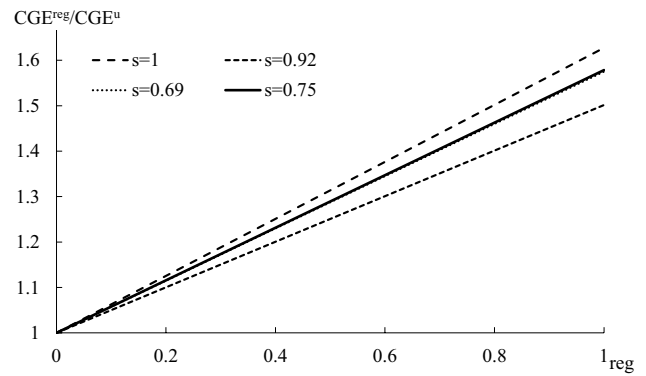


Fig. 9 CGE with regeneration

is determined by the composition of the gasification products shown in Fig. 3a.

The ratio of CGE with regeneration to CGE without it was determined:

$$CGE^{reg} = 1 + \left(1 - \frac{CGE}{100}\right) \cdot reg, \quad (20)$$

where  $CGE_{reg}$  is CGE with regeneration (%);  $reg$  refers to the degree of regeneration. The results are presented in Fig. 9.

With a technically achievable degree of waste gas heat recovery  $reg = 0.8$ . CGE increases up to 70%.

### 3.6 Comparison of the results with literature data

Comparison of the results with literature data is presented in Table 4.

It can be seen from the table that the optimized gasifier under study produces syngas with the highest heating value among all BFB and is second only to CFB. This is achieved by allocating a separate section for gasification and a separate section for combustion. The part of the coal that burns in the combustion section transfers heat to the gasification section through the central tube wall, with the inert material and with the char. However, the  $CO_2$  that is formed in this process does not mix with the syngas and is removed by a separate stream of combustion products.

CGE of the studied gasifier is inferior only to one of BFB. This is due to the fact that in the BFB there is air heating up to  $300\text{--}350 \text{ }^\circ\text{C}$ , which allows you to burn less coal to produce the heat necessary for endothermic gasification reactions.

The relatively low  $X_C$  in the studied gasifier is again explained by the division into two sections. A fairly large amount of carbon is burned in the combustion section. However, in this case, a relatively hot gas flow is formed in the combustion section, which can be used to heat the primary air of the gasifier, or to transfer it to external consumers, for example, to a gas turbine or heat recovery steam generator.

**Table 4** Comparison of the results with literature data

Gasifier	T, °C	$Q_s^g$ , MJ/m <sup>3</sup>	CGE, %	$X_C$ , %
SFB (Xiao et al. 2006)	940–950	3.6–4.7	46–59	62–79
CFB (Ju et al. 2010)	970–1030	2.9–5.8	42–73	46–93
BFB-1-1 (Tomeczek et al. 1987)	840–900	3.4–4.5	–	55–63
	845–920	2.9–4.2	–	55–65
BFB-1-1 (Lee et al. 2002)	750–900	1.7–2.8	17–22	30–45
BFB-1-1 (Engelbrecht et al. 2010)	948	2.8	–	85.9
	978	2.9	–	67
BFB-1-1 (Ocampo et al. 2012)	812–872	2.7–3.3	–	47–69
BFB-1-1 (Chavan et al. 2012)	860–932	2.19–5.17	–	58–92
BFB-1-1 (Vijay Kumar et al. 2017)	922–1040	2.84–4.81	61–78	75–84
BFB-1-1 (Gupta and De 2022)	811–895	1.77–3.0	29–46	71–85
BFB-1-2 without optimization	770–990	3.6–4.5	42–42.3	53–62
BFB-1-2 with optimization	770–990	5.2–5.34	42.5–50	49–57

Such a scheme makes it possible to recover part of the heat and increase the efficiency of the gasifier up to 70%, as shown in the previous paragraph. In another two-section gasifier (Khan and Wang 2013), discussed in the introduction, the unburned carbon must be disposed of in a separate pulverized coal boiler, which complicates and increases the cost of the plant layout as a whole. In our case, it is possible to burn almost all carbon of the fuel due to the high flow rate of secondary and tertiary air in the combustion section, which makes the plant layout simpler and cheaper.

## 4 Conclusions

(1) Using a newly developed experimental setup, the features and advantages of an autothermal single-casing atmospheric subbituminous coal fluidized bed air-blown gasifier, combining a combustion section and a gasification section, with mixing of the dispersed phase (inert material, char) and heat exchange between them through an annular transfer device, were revealed.

(2) To increase the efficiency of the gasifier, an experimental-computational method has been developed for finding the conditions for optimal operation, combining changes to the geometry of the annular flow and regulation of the primary air for gasification. A simple and reliable multizone thermodynamic calculation model makes it possible to predict the composition of char and syngas in the gasification section with acceptable accuracy. This method confirmed that a two-section fluidized bed gasifier can provide efficient gasification of solid fuels and is suitable for use in small-scale cogeneration plants.

(3) A two-parameter optimization task is solved, which is carried out step-by-step: in terms of the design parameter  $s$  and in terms of the regime parameter  $\alpha$ . Optimization at the first step increased the heating value from 3.6 to 4.5 MJ/m<sup>3</sup> (by 25%) and the CGE from 38.2% to 42.3% (by 10.7%). Optimization at the second step further increased the heating value from 3.6 to 5.3 MJ/m<sup>3</sup> (by 27%) and the CGE from 38.2% to 42.5% (by 11.2%). The overall increase in the syngas heating value is 3.6–5.34 MJ/m<sup>3</sup> (by 48%) and the CGE is 38.2%–50.0% (by 31%). With heat regeneration of 0.8, CGE increases to 70%. Optimal gasifier operating parameters:  $s = 0.92$  ( $d = 0.262$  m),  $B = 25.4$  kg/h,  $V_1 = 34.5$  m<sup>3</sup>/h ( $\alpha_g = \alpha_c$ ).

**Acknowledgements** The research funding from the Ministry of Science and Higher Education of the Russian Federation (Ural Federal University Program of Development within the Priority-2030 Program) is gratefully acknowledged.

## Declarations

**Competing interests** The authors declare that they have no known competing financial interests or personal relationships that could have appeared to influence the work reported in this paper.

**Open Access** This article is licensed under a Creative Commons Attribution 4.0 International License, which permits use, sharing, adaptation, distribution and reproduction in any medium or format, as long as you give appropriate credit to the original author(s) and the source, provide a link to the Creative Commons licence, and indicate if changes were made. The images or other third party material in this article are included in the article's Creative Commons licence, unless indicated otherwise in a credit line to the material. If material is not included in the article's Creative Commons licence and your intended use is not permitted by statutory regulation or exceeds the permitted use, you will need to obtain permission directly from the copyright holder. To view a copy of this licence, visit <http://creativecommons.org/licenses/by/4.0/>.

## References

- Alamia A, Larsson A, Breitholtz C, Thunman H (2017) Performance of large-scale biomass gasifiers in a biorefinery, a state-of-the-art reference. *International Journal of Energy* 41:2001–2019
- Antonelli J, Lindino CA, Bariccatti RA, Souza SNM, Lenz AM (2017) Lead adsorption and subsequent gasification with *Pinus elliottii* waste. *Management of Environmental Quality: an International Journal* 28:839–850
- Beenackers AACM, Maniatis K (1996) Gasification technologies for heat and power from biomass. In: *Proceedings of the 9th European Bioenergy Conference, Copenhagen, Denmark, 24–27 June; vol 1*, pp 228–259
- Biagini E, Barontini F, Tognotti L (2016) Development of a bi-equilibrium model for biomass gasification in a downdraft bed reactor. *Biores Technol* 201:156–165
- Bläsing M, Müller M (2013) Release of alkali metal, sulphur, and chlorine species from high temperature gasification of high- and low-rank coals. *Fuel Process Technol* 106:289–294
- Castro RR, Brequigny P, Mounaïm-Rousselle C (2022) A multiparameter investigation of syngas/diesel dual-fuel engine performance and emissions with various syngas compositions. *Fuel* 318:123736
- Chavan P, Datta S, Saha S, Sahu G, Sharma T (2012) Influence of high ash indian coals in fluidized bed gasification under different operating conditions. *Solid Fuel Chem* 46(2):108–113
- Cloete S, Giuffrida A, Romano M, Chiesa P, Pishahang M, Larring Y (2018) Integration of chemical looping oxygen production and chemical looping combustion in integrated gasification combined cycles. *Fuel* 220:725–743
- Ding N, Zhang C, Luo C, Zheng Y, Liu Z (2015) Effect of hematite addition to CaSO<sub>4</sub> oxygen carrier in chemical looping combustion of coal char. *RSC Adv* 5:56362–56376
- Ding L, Yoshikawa K, Fukuhara M, Kowata Y, Nakamura S, Xin D, Muhan L (2018) Development of an ultra-small biomass gasification and power generation system: Part 2. Gasification characteristics of carbonized pellets/briquettes in a pilot-scale updraft fixed bed gasifier. *Fuel* 220:210–219
- Ding L, Yang M, Dong K, Vo DV, Hungw D, Ye J, Ryzhkov A, Yoshikawa K (2022) Mobile power generation system based on biomass gasification. *Int J Coal Sci Technol* 9:34
- Donskoi IG, Marinchenko AY, Cler AM, Ryzhkov AF (2015) Optimizing modes of a small-scale combined-cycle power plant with atmospheric-pressure gasifier. *Thermophys Aeromech* 5:639–646
- Du S, Yuan S, Zhou Q (2021) Numerical investigation of co-gasification of coal and PET in a fluidized bed reactor. *Renew Energy* 172:424–439
- Dubin AM, Shcheklein SE (2017) Mini coal-fired CHP plant on the basis of synthesis gas generator (CO + H<sub>2</sub>) and electrochemical current generator. *Int J Hydrogen Energy* 42:26048–26058
- Dubin YV, Yazykov NA, Reshetnikov SI, Yakovlev VA (2021) Catalytic combustion of sulfur-containing liquid fuels in the fluidized bed: Experiment and modeling. *J Ind Eng Chem* 93:163–169
- Emiola-Sadiq T, Wang J, Zhang L, Dalai A (2021) Mixing and segregation of binary mixtures of biomass and silica sand in a fluidized bed. *Particuology* 58:58–73
- Engelbrecht AD, Everson RC, Neomagus HWPJ, North BC (2010) Fluidized bed gasification of selected South African coals. *J Southern Afr Inst Min Metall* 110(5):225–230
- Figuerola JEJ, Ardila YC, Filho RM, Maciel MRW (2017) Biomass gasification optimization: semi-pilot scale 2 kg/h of bagasse in fluidized bed reactor. *Chem Eng* 57:937–942
- Gorokhovski M, Karpenko EI, Lockwood FC, Messerle VE, Trusov BG, Ustimenko AB (2005) Plasma technologies for solid fuels: experiment and theory. *J Energy Inst* 78:157–171
- Gupta S, De S (2022) An experimental investigation of high-ash coal gasification in a pilot-scale bubbling fluidized bed reactor. *Energy* 244:122868
- Hamelinck CN, Faaij APC, Uil H, Boerrigter H (2004) Production of FT transportation fuels from biomass: technical options, process analysis and optimization, and development potential. *Energy* 29:1743–1771
- Hansen CJ, Bower J (2004) An economic evaluation of small-scale distributed electricity generation technologies. Oxford Institute for Energy Studies & Dept. of Geography, Oxford University, Oxford
- Hasegawa T (2010) Gas turbine combustion and ammonia removal technology of gasified fuels. *Energies* 3:335–449
- Hedenskog M (2014) Gasification of forest residues in a large demonstration scale – the Gobigas-Project. International seminar on gasification. The Swedish gas technology center. Malmö, Sweden
- Ismail TM, Shi M, Xu J, Chen X, Wang F, El-Salam MA (2020) Assessment of coal gasification in a pressurized fixed bed gasifier using an ASPEN plus and Euler–Euler model. *Int J Coal Sci Technol* 7(3):516–535
- JANAF (1985) Thermochemical Tables (Third Edition). *J. Phys. Chem. Ref. Data* vol.14 Suppl. No.1. [www.nist.gov/sites/default/files/documents/srd/JPCRD302001475p.pdf](http://www.nist.gov/sites/default/files/documents/srd/JPCRD302001475p.pdf). Accessed 22 Dec 2018
- Jiang P, Mahmud Parvez A, Meng Y, Dong X, Xu M, Luo X, Shi K, Wu T (2021) Novel two-stage fluidized bed-plasma gasification integrated with SOFC and chemical looping combustion for the high efficiency power generation from MSW: a thermodynamic investigation. *Energy Convers Manag* 236:114066
- Jiao Z, Liu L, Zhao Y, Chen X, Qiu P (2021) Study on reactivity and synergy behavior of cogasification between biomass char and coal char. *Energy Fuels* 35:341–350
- Ju F, Chen H, Yang H, Wang X, Zhang S, Liu D (2010) Experimental study of a commercial circulated fluidized bed coal gasifier. *Fuel Process Technol* 91(8):818–822
- Kaneko S, Hashimoto T, Furuya T, Uchida S (1997) Operational results of 200 t/d IGCC pilot plant in Nakoso. *Mater High Temp* 14:87–94
- Khan J, Wang T (2013) Implementation of demoinsturation and devolatilization model in multi-phase simulation of hybrid entrained flow and fluidized bed mild gasifier. *Int J Clean Coal Energy* 2:35–53
- Kumari P, Mohanty B (2020) Hydrogen-rich gas production with CO<sub>2</sub> capture from steam gasification of pine needle using calcium oxide: experimental and modeling study. *Int J Energy Res* 44:6927–6938
- Laugwitz A, Meyer B (2014) New frontiers and challenges in gasification technologies. In: Nikrityuk PA, Meyer B (eds) *Gasification processes: modeling and simulation*. Wiley, Hoboken
- Leckner B (2016) Developments in fluidized bed conversion of solid fuels. *Therm Sci* 20:1–18
- Lee W-J, Kim S-D, Song B-H (2002) Steam gasification of an Australian bituminous coal in a fluidized bed. *Korean J Chem Eng* 19(6):1091–1096
- Li B, Lyu Z, Zhu J, Han M, Sun Z (2021) Study on the operating parameters of the 10 kW SOFC-CHP system with syngas. *Int J Coal Sci Technol* 8(4):500–509
- Luckos A, Bunt JR (2011) Pressure-drop predictions in a fixed-bed coal gasifier. *Fuel* 90:917–921
- Ma J, Tian X, Wang C, Zhao H, Liu Z, Zheng C (2021) Fate of fuel-nitrogen during in situ gasification chemical looping combustion of coal. *Fuel Process Technol* 215:106710
- Matsuoka K, Kuramoto K, Hosokai S, Sato H, Tsuboi Y (2021) Reducing tar emissions during coal gasification by optimizing the cracking/reforming over char in a fluidized bed. *Energy Fuels* 35:5955–5962

- Meng N, Leung DYC, Leung MKH, Sumathy K (2006) An overview of hydrogen production from biomass. *Fuel Process Technol* 87:461–472
- Messerle VE, Ustimenko AB, Lavrichshev OA (2017) Plasma coal conversion including mineral mass utilization. In *Fuel* 203:877–883
- Ocampo A, Arenas E, Chejne F, Espinel J, Londoo C, Aguirre J, Perez JD (2003) An experimental study on gasification of Colombian coal in fluidised bed. *Fuel* 82(2):161–164
- Pérez-Astray A, Adánez-Rubio I, Mendiara T, Izquierdo M, Abad A, Gayán P, de Diego L, García-Labiano F, Adánez J (2019) Comparative study of fuel-N and tar evolution in chemical looping combustion of biomass under both iG-CLC and CLOU modes. *Fuel* 236:598–607
- Perrone D, Castiglione T, Morrone P, Pantano F, Bova S (2023) Numerical and experimental assessment of a micro-combined cooling, heating, and power (CCHP) system based on biomass gasification. *Appl Therm Eng* 219:119600
- Ryzhkov AF, Kostyunin VV, Silin VE, Dubinin AM (2004) Comparative analysis of mechanisms of thermal-chemical activation of solid fuel. *Khim Fiz* 23:9–13
- Ryzhkov AF, Bogatova TF, Lingyan Z, Osipov PV (2016) Development of entrained-flow gasification technologies in the Asia-Pacific region (review). *Therm Eng* 63:791–801
- Ryzhkov A, Bogatova T, Gordeev S (2018) Technological solutions for an advanced IGCC plant. *Fuel* 214:63–72
- Sheng C, Xu M, Zhang J, Xu Y (2000) Comparison of sulphur retention by coal ash in different types of combustors. *Fuel Process Technol* 64:1–11
- Sua F, Hamanak A, Itakura K, Zhang W, Deguchi G, Sato K, Takahashi K, Kodam J (2018) Monitoring and evaluation of simulated underground coal gasification in an ex-situ experimental artificial coal seam system. *Appl Energy* 223:82–92
- Suárez-Almeida M, Gómez-Barea A, Pfeifer C, Leckner B (2021) Fluid dynamic analysis of dual fluidized bed gasifier for solar applications. *Powder Technol* 390:482–495
- Tomeczek J, Kudzia W, Gradonó B, Remarczyk L (1987) The influence of geometrical factors and feedstock on gasification in a high temperature fluidised bed. *Can J Chem Eng* 65(5):785–790
- Tsuji T, Uemaki O (1994) Coal gasification in a jet-spouted bed. *Can J Chem Eng* 72(3):504–510
- Vijay Kumar K, Bharath M, Raghavan V, Prasad BVSSS, Chakravarthy SR, Sundararajan T (2017) Gasification of high-ash Indian coal in bubbling fluidized bed using air and steam—an experimental study. *Appl Therm Eng* 116:372–381
- Wang X, Li Y, Zhang W, Zhao J, Wang Z (2020) Simultaneous SO<sub>2</sub> and NO removal by pellets made of carbide slag and coal char in a bubbling fluidized-bed reactor. *Process Saf Environ Prot* 134:83–94
- Wiatowski M, Kapusta K, Nowak J, Szyja M, Basa W (2021) An ex-situ underground coal gasification experiment with a siderite inter-layer: course of the process, production gas, temperatures and energy efficiency. *Int J Coal Sci Technol* 8(6):1447–1460
- Xiao R, Zhang M, Jin B, Huang Y, Zhou H (2006) High-temperature air/steam-blown gasification of coal in a pressurized spout-fluid bed. *Energy Fuels* 20(2):715–720
- Xiaorui L, Xudong Y, Guilin X, Yiming Y (2021) NO emission characteristic during fluidized combustion of biomass with limestone addition. *Fuel* 291:120264
- Yan J, Zheng X, Lu X, Liu Z, Fan X (2021) Enhanced combustion behavior and NO<sub>x</sub> reduction performance in a CFB combustor by combining flue gas recirculation with air-staging: Effect of injection position. *J Energy Inst* 96:294–309
- You S, Ok YS, Tsang DCW, Kwon EE, Wang C-H (2018) Towards practical application of gasification: a critical review from syngas and biochar perspectives. *Crit Rev Environ Sci Technol* 48:1165–1213

**Publisher's Note** Springer Nature remains neutral with regard to jurisdictional claims in published maps and institutional affiliations.